International Journal of Advanced Research in Physical Science (IJARPS)
Volume 9, Issue 4, 2022, PP 19-33
ISSN No. (Online) 2349-7882
www.arcjournals.org

Laser-Induced Sputtering (Ablation) of Matter: Retrospective and Perspective

Petro P. Trokhimchuck*

Anatoliy Svidzinskiy Department of Theoretical and Computer Physics, Lesya Ukrayinka Volyn' National University, 13 Voly Avenue, 43025, Lutsk, Ukraine

Corresponding Author:** ***Petro P. Trokhimchuck, *Anatoliy Svidzinskiy Department of Theoretical and Computer Physics, Lesya Ukrayinka Volyn' National University, 13 Voly Avenue, 43025, Lutsk, Ukraine*

Abstract: *Main peculiarities of laser-induced sputtering (ablation) of matter are discussed. It is shown that there are three types of processes for which photochemical, plasma and thermal phenomena are predominant. Moreover, these processes have a cascade nature. Corresponding experimental data, models and theories are represented. Conditions for the regimes of laser irradiation and irradiated matter, which are necessary for the creation and observation the proper regime of laser-induced sputtering are formulated and discussed. Questions about possible observation these phenomena by methods of Relaxed optics are analyzed.*

Keywords: *sputtering, laser irradiation, ablation, Relaxed Optics, cascade processes, laser technology, saturatin of excitation.*

1. INTRODUCTION

Problem of the observation the laser-induced sputtering of matter is one of the central questions of modern optoelectronic technology [1 – 19]. In parallel, before this, there is also the term ablation, which roughly speaking means the same thing. The term sputtering is used when considering the impact of laser radiation, as a stream of particles, when compared with other types of irradiation (ion, electron, etc.) [1, 2].The removal of a material substance from its surface using laser radiation is called laser ablation [1, 2]. We will consider this issue a little more broadly, so herein after we will call this process laser-induced sputtering.

In general, these processes have a cascade nature. Depending on the irradiation conditions, there can be the following cascades of processes [3]:

1. Irradiation – heating of the material – sublimation;

2. Irradiation – material melting – evaporation;

3. Irradiation – a cascade of formation of intermediate lower-symmetry phases – sublimation.

It is very rough classification, but it allow consider all types of laser ablation from a single point of view.

For example, the number of intermediate phases for silicon is 4 if only crystalline ones and 11 together with quasi-crystalline ones are taken into account [20, 21]. For polymers, this number is much higher and requires additional research [21].

Laser-induced processes have more soft nature [2]. Therefore, we must use the methods of modeling, which are allow to explain the possible chains intermediate phase transformations [2]. In this case we must use the cascade model of excitation of proper chemical bonds in the regime of saturation of excitation [21 – 26]. Roughly speaking, the laser-induced surface sputtering of irradiated matter without melting must be realized for the regime of irradiation, which is equal of sum the chemical bonds of surface atoms. As rule, this value is equal the half of Seitz energy (sum of all nearest chemical bonds of corresponding atoms in crystal lattice) [27]. In order of magnitude, this value corresponds to the sublimation energy of the irradiated material. In this case, we must select regimes of irradiation, which generating cascade "quantum" short-range actions, because the transition to long-range action may be cause of melting the irradiated matter.

The pure laser sublimation (sputtering) method is more preferable for obtaining the micro-hole drilling of stainless steel using short laser pulses [15], because it does not leave molten droplets on the irradiated surface, in addition, the holes themselves have a more even border. This method may be used for the laser-induced sublimation the indium antimonite after stationary CO_2-laser irradiation [23]. The experimental data were represented for multipulses regimes of irradiation too [4 – 11, 14, 16].

In whole methods of laser-induced sputtering may be used for the cleaning the surfaces of materials and their corresponding profiles, while laser methods can be used for samples with a significantly smaller size [4 – 16].

We use physical-chemical, thermal and plasma methods for modeling the represented experimental data [2, 3, 16, 28].

2. EXPERIMENTAL DATA

The laser-induced evaporation (sputtering) may be realized with two channels: evaporation from a melt (ablation) and evaporation from a solid state (sublimation) [23].

Sublimation of indium antimonite after irradiation of stationary CO_2 laser (wavelength 10,6 μm, effective density of power ~ 60 – 80 $W{\cdot}cm^{-2}$, time of irradiation ~ 10 – 15 s, uniformity of irradiation ~ 10 percents on the area with diameter 6 mm) [23]. Irradiated samples have cruciform (Hall samples) with sizes $2{\cdot}4$ mm^2 (main sample) and two Hall contact with area $0.5{\cdot}1$ mm^2 [23, 27]. The color of the samples during irradiation was as follows: dark red – bright red – dark red light. During this, it evaporated and only Hall contacts remained, with which it was attached to the tripod on which the irradiation took place. In this case, there was no melting of the irradiated material. Absorption index of 10.6 μm radiation for *InSb* is equaled ~10 cm^{-1} [23].

The main experimental data, which are demonstrate the cascade nature of laser-induced ablation processes are represented on Fig. 1 – Fig. 3 [8, 11].

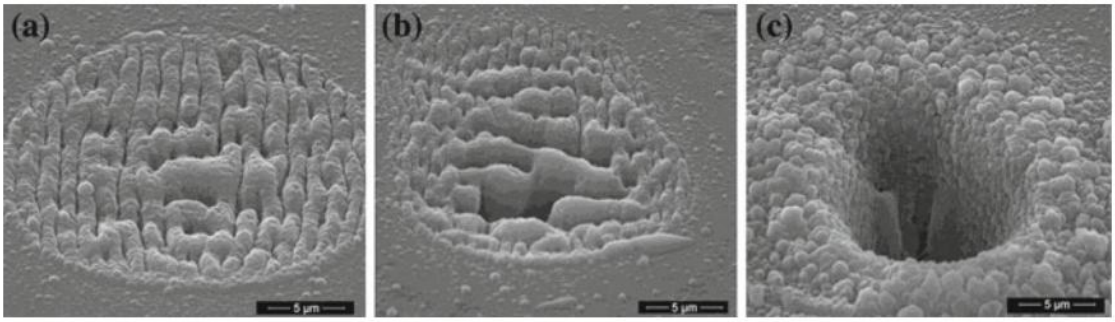

Fig1. *Target spot area morphology for the case of 'mild ablation' after: (a) Several pulses; (b) Ten of pulses; (c) Hundred of pulses (Si target, 7 ps pulse duration, 1064 nm wavelength) [11].*

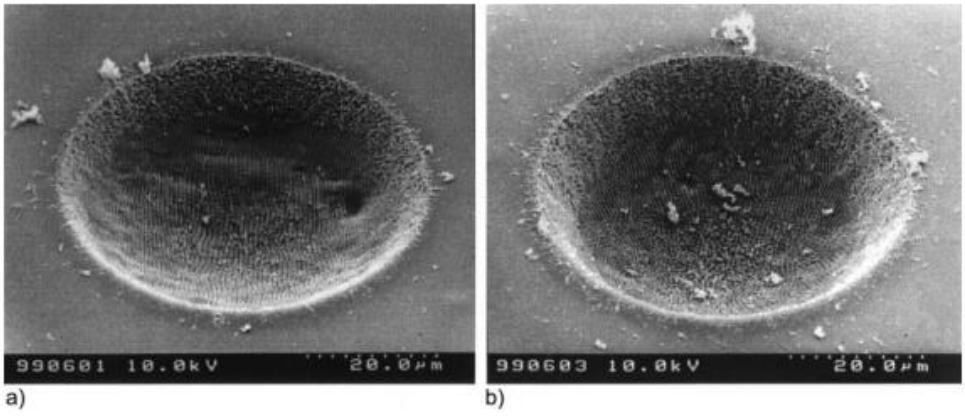

Fig2. *SEM pictures of irradiated areas, obtained with the 50 pulses: a) linear polarization (vector of electric field is parallel to the periodic structure); b) circular polarization of the laser pulses (fluence 1.3 $J{\cdot}cm^{-2}$, ,duration of pulse 150 fs, wavelength 800 nm, focal length 60 mm, visual angle 60º) [11].*

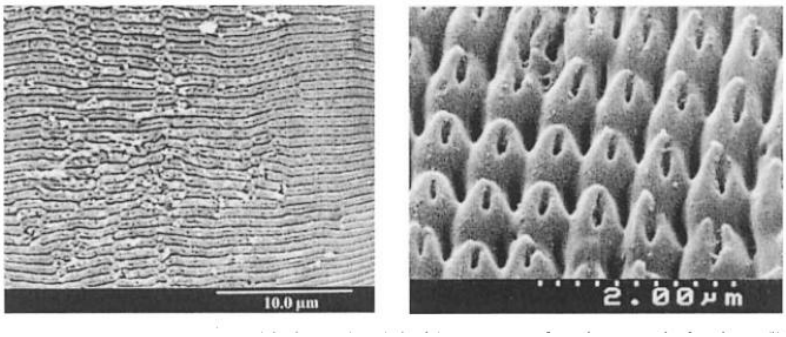

Fig3. *Femtosecond laser ablation of polyimide (PI). (Left) Linear polarization. (Right) Circular polarization. Fluence 1.3 J·cm^{-2}, number of pulses 50, duration of pulse 150 fs [8].*

The ablation depth was measured in the following way: for veach interpulse delay, a series of 10 craters was drilled, with an increasing number of applied DPs, as shown in Fig. 4. The depth of each crater was measured using optical microscopy by focusing on the samples surface and the crater bottom [5]. According to the linear increase of crater depth z with the number of DPs n_{1as}, the ablation depth was deduced from the slope $\Delta z / \Delta n_{1as}$.

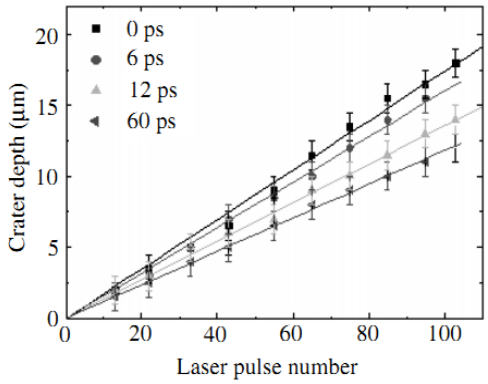

Fig4. *Crater depth versus of applied dubble pulses for ablation of copper with various interpulse delays. The ablation depth (per double pulse) was deduced from the slope [5].*

Laser structures of LCO can be realized via classical laser direct ablation or via self-organized structuring (Fig. 5. [5]).

The demands for high precise micro-holes are increasing with the increasing of application range, therefore traditional mechanical drilling is slightly applicable. On the other hand, laser drilling using continuous-wave lasers is accompanied with the formation of melting layer and due to its uncontrolled redeposition – recast layer. The best way of overcoming main laser drilling disadvantages is laser pulse shortening, so that only material ablation by nonlinear absorption takes place [80]. Such material ablation could be achieved by using of picosecond or even femtosecond laser sources because ablation of pulsed laser radiation depends on the length of the respective pulse. Different pulse lengths have different etching mechanisms during removal of the material, and the shape of the material surface will be different after the removal process.

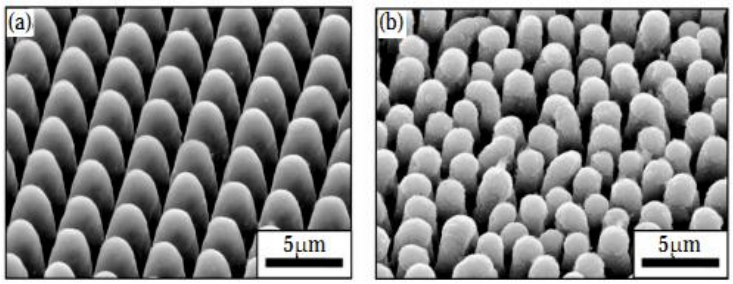

Fig5. *SEM images of laser-structured $LiCoO_2$ thin films using mask imaging (a) with a laser fluence of 3 J/cm^2 and self-organized structures and (b) with laser fluences of 0.5 J/cm^2 and 2 J/cm^2. Sixty laser pulses at a repetition rate of 100 Hz were applied [5].*

Although studies on micro-hole drilling by short pulsed lasers has received much attention, drilling of high precise micro-holes with minimal or no thermal damage still remains a major challenge [2, 15].

In work [15] micro-hole drilling was processed using TRUMPF TruMicro 5000 picosecond laser. The wavelength of the laser was 515 *nm* with a pulse width of 10 *ps* at 400 *kHz* pulse repetition frequency. The power density was $5.72 \cdot 10^5$ $W \cdot cm^{-2}$, and equivalence laser fluence was 1.43 $J \cdot cm^{-2}$. Micro-holes were received in steel SAE-304 (Fig. 6) [15]

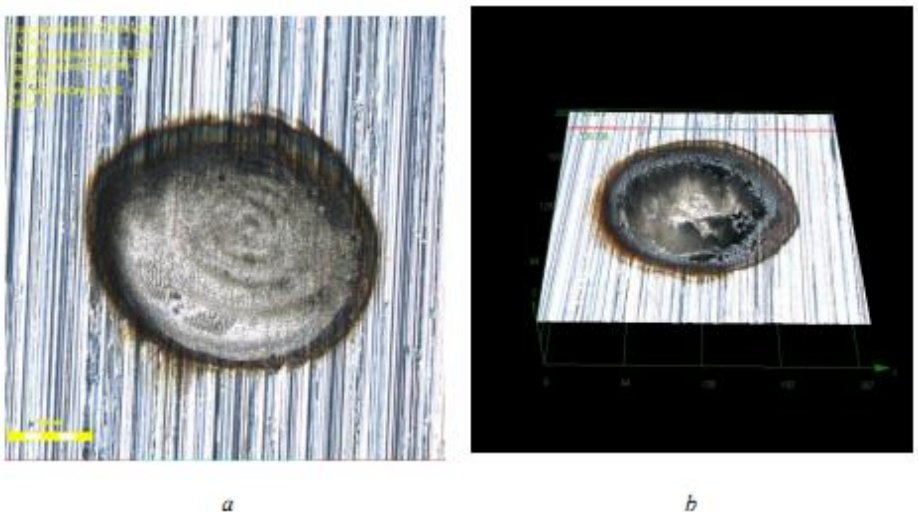

a *b*

Fig6. *Micro-holes drilled in stainless steel using picosecond laser: a - 30 shots, 2D view; b –190 shots, 3D – view [15].*

Line profiles of drilled micro-holes fordifferent amount of shots is represented on Fig. 7 a) [15]. Depth of the hole drilled using picosecond laser for different number of pulses was researched too (Fig. 7 b)) [15].

As seen from Fig. 7 b) the dependence of the depth of holes tends to saturate. This is obviously due to the increase in light reflection compared to previous pulses.

In order to avoid dross (Fig. 6), it is advisable to choose the modes of laser irradiation such that the main processes are sublimation of the irradiated material. This mode is easy to choose, since the binding energy of near-surface atoms is 1.2 - 2 times less than that of bulk atoms, while we will have laser-induced sputtering with a solid rather than a liquid phase.

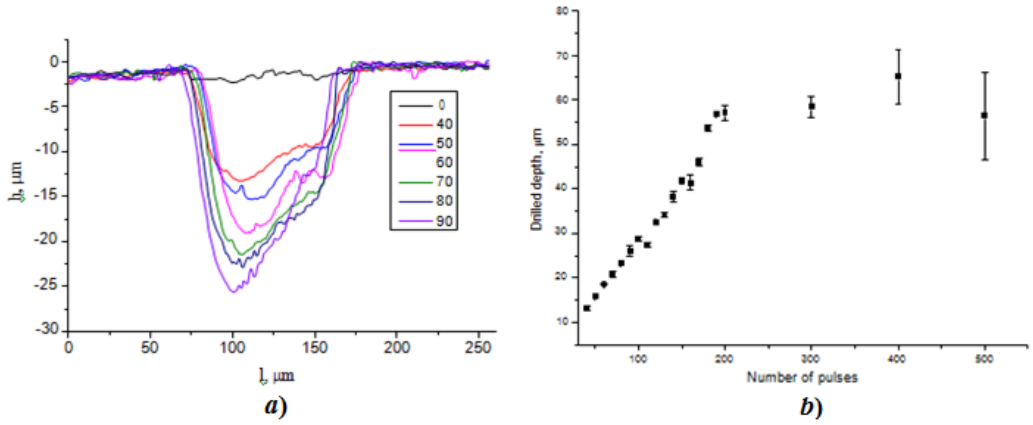

Fig7. ***a)*** *Line profiles of drilled micro-holes fordifferent amount of shots [15];* ***b)*** *Depth of the hole drilled using picosecond laser for different number of pulses [15].*

Removal rate, air shock, and ablative recoil pressure parameters were measured as a function of laser intensity I_{peak} during nanosecond laser ablation of graphite were researched in [16]. Surface vaporization of molten graphite at low intensities $I_{peak} < 0.15$ $GW \cdot cm^2$ was observed to transform into its near-critical phase explosion (intense homogeneous boiling) at the threshold intensity $I_{PE} \approx 0.15$ $GW \cdot cm^2$ in the form of a drastic, correlated rise of removal rate, air shock, and ablative recoil

pressure magnitudes. Just above this threshold ($I_{peak} \geq 0.25$ GW/cm^2), the explosive mass removal ended up with saturation of the removal rate, much slower increase of the air and recoil pressure magnitudes, and appearance of a visible surface plasma spark. In this regime, the measured far-field air shock pressure amplitude exhibits a sublinear dependence on laser intensity $\left(\sim I_{peak}^{4/9}\right)$, while the source plasma shock pressure demonstrates a sublinear trend $\left(\sim I_{peak}^{3/4}\right)$ both indicating the subcritical character of the plasma. Against expectations, in this regime the plasma recoil pressure increases versus I_{peak} superlinearly $\left(\sim I_{peak}^{1.1}\right)$, rather than sublinearly $\left(\sim I_{peak}^{3/4}\right)$, with the mentioned difference related to the intensity-dependent initial spatial plasma dimensions within the laser waist on the graphite surface and to the plasma formation time during the heating laser pulse (overall, the pressure source effect). The strict coincidence of the phase explosion, providing high (*kbar*) hydrodynamic pressures of ablation products, and the ignition of ablative laser plasma in the carbon plume may indicate the ablative pressure-dependent character of the underlying optical breakdown at the high plume pressures, initiating the plasma formation. The experimental data evidence that the spatiotemporal extension of the plasma in the laser plume and ambient air during the heating laser pulse support by fast lateral electron and radiative heat conduction (laser-supported combustion wave regime), rather than by propagation of a strong shock wave (laser-supported detonation wave regime).

In these experiments we performed laser ablation of millimeter-thick polycrystalline graphite plates (mass density $p_0 \approx 1.7$ g/cm^3) [16]. A primary laser source was a frequency- doubled Nd:YAG laser (LTIPCh-412) with a lasing wavelength $\lambda \approx 532$ *nm*, laser pulse full width at a half maximum (FWHM) $\tau_i \approx 25$ *ns*, and a maximum pulse energy in the TEM_{00} mode ≈ 50 *mJ* at a repetition rate of 12.5 *Hz*. The 532 *nm* laser pulses were focused using a silica lens (focallength $f \approx 40$ *cm*) into focal spots $w_0 \approx 40 - 150$ μm (at the $1/e$ level) and their energies were monitored by means of a thermocouple energy meter.

Simultaneously, the related dependence pressure $P_{air}(I_{peak})$ also ex- hibits the same initial region of a non-linear pressure variation prior its succeeding sharp rise near the same intensity value $I_{PE} \approx 0.15$ GW/cm^2 (Fig. 8 *a*)) [16].

Meanwhile, in this intensity range the experimentally measured air transit times t_{tr} for the pressure perturbations in air show supersonic average propagation velocities C_{ave} (in air, the sound velocity equals to 0.346 *km/s* at the normal conditions [16]) (Fig. 8 *b*)), calculated simply dividing the 23-*mm* long propagation distance l_{air} by t_{tr}: $C_{ave}=l_{air}/t_{tr}$. In the far-field air region, where the ultrasonic data acquisition takes place, the air pressure perturbations propagate in the form of a spherical (diffracted) wave with the initial radius R_S, which is proportional to the waist radius (see the similarity of P_{air}/w_0 dependences on I_{peak} for I_{peak}= 0.2 – 50 GW/cm^2 and different laser spot radii w_0 in inset to Fig. 8 *a*)), and the almost hyperbolic radial pressure variation [16]

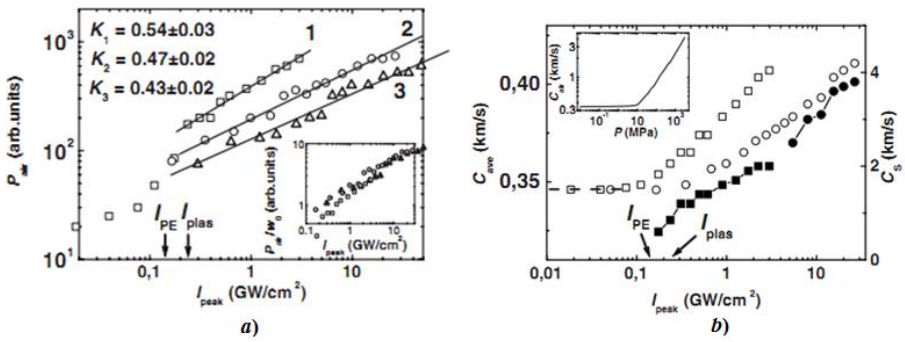

Fig8. ***a)*** *Air pressure P_{air} for the different laser spot radii w_0 [150 (squares), 55 (circles) and 40 (triangles) μm] versus I_{peak} with the linear fitting curves 1–3 (slopes $K_{1,2,3}$). Inset: the same, but normalized P_{air}/w_0 curves versus I_{peak}.* ***b)*** *Average (light marks, C_{ave}, left axis) and initial (dark marks, C_S, right axis) for the different laser spot radii w_0 [150 (squares) and 55 (circles) μm] versus I_{peak}. Inset: pressure dependence of sound velocity in air (after [16]).*

$$P(r) = P_S\left(\frac{R_s}{r}\right), \tag{1}$$

where P_S is the initial (source) pressure. According to the pressure dependence of the longitudinal sound velocity in air C_{air} [130] (Fig. 8 b)), inset), such diffraction results in gradually decelerating radial motion of the pressure waves from the ablative source on the graphite surface and resulting in the supersonic average propagation velocities C_{ave} reading as

$$C_{ave} = l_{air}\left\{\int_0^{l_{air}} \frac{dr}{C_{air}[P(r)]}\right\}^{-1}. \tag{2}$$

Hence, the measured average propagation velocities C_{ave} in air can be converted into the initial ablative source pressures P_S and shock wave velocities C_S. The resulting dependence $P_S(I_{peak})$ in Fig. 9a) demonstrates drastic rise at $I_{peak} \geq I_{PE}$, as well as the related $X(I_{peak})$ and $P_{rec}(I_{peak})$ curves, with theevaluated ablative pressure values P_S in reasonable agreement with the independently estimated pressure values P_{rec} [ion]; the discrepancy by the factor of 2 may result from redeposition of the ablated material, significantly decreasing its removal rate [16]. The derived P_S magnitudes at $I_{peak} \approx I_{PE}$ are close to the near-critical vapor pressure values of graphite (Fig. 9a)), as well as similar (a few kbar) ablative pressures of aluminum near its laser-induced phase explosion threshold [16], indicating the onset of the near-critical surface phase explosion.

Interestingly, at higher laser intensities $0.25\ GW/cm^2 < I_{peak} < 0.6\ GW/cm^2$ the removal rate X saturates at the monotonously increasing P_{rec} [ion] and P_S (Fig. 9a)) pressures, i.e., the abovementioned correlation between the mass removal and near-surface plume/plasma pressure quantities fails. The saturation of X indicates that laser ablation is com- pletely screened (shielded) by absorption in the dense abla- tive plume, while this absorption produces an extra pressure of the plume on the target, which may originate from an expanding ablative laser plasma, emerging in the plume at $I_{peak} \geq 0.3 GW/cm^2 > I_{PE}$ (Fig. 9 b)(b)). By the way, on this and previous images (Figs. 9 b)(a) and 9 b)(b)), corresponding to $I_{peak} \geq I_{PE}$, light tracks (fountains) of micrometer sized droplets are visible in the laser plumes after the preceding surface phase explosions [16].

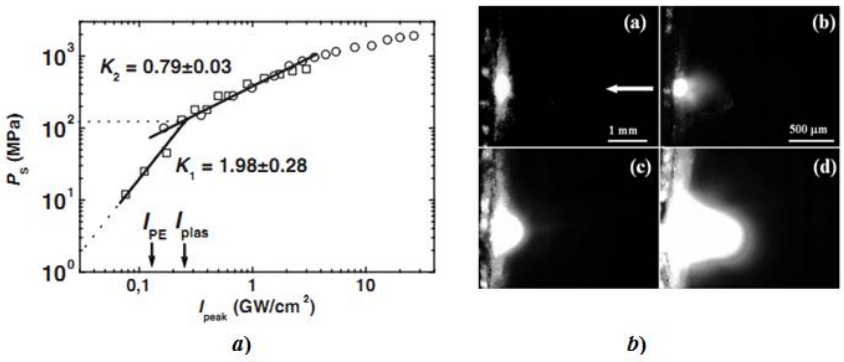

a) *b)*

Fig9. ***a)*** *Plume/plasma pressure P_S for w_0 = 270 (squares) and 95 (circles) µm versus I_{peak} with the low-($I_{peak} < I_{PE}$) and high- intensity ($I_{peak} > I_{plas}$) linear fitting curves 1–2 (slopes $K_{1,2}$). The dotted horizontal and inclined lines denote the maximum ablation pressure value of ≈1140 bar achieved at $I_{peak} \approx I_{plas}$ prior dense plasma formation, and the estimate of the carbon vapor pressure upon its laser melting at $I_{peak} \approx I_{abl} \approx 0.03\ GW/cm^2$, respectively.* ***b)*** *Optical images of single-shot ablative carbon plasmas at $I_{peak} \approx 0.15$ (a), 0.3 (b), 4 (c) and 14 (d) GW/cm^2 [the scale bar is similar for images (b)–(d)]. The arrow shows the laser incidence direction.*

3. MODELING AND DISCUSSIONS

The problem of particle sputtering may be connected with thermodynamic concept of sublimation but although it also has significant differences due to the processes of interaction of specific particles with the environment.

Sublimation is the transition of a substance directly from the solid to the gas state, without passing through the liquid state [28]. Sublimation is an endothermic process that occurs at temperatures and pressures below a substance's triple point in its phase diagram, which corresponds to the lowest

pressure at which the substance can exist as a liquid. The reverse process of sublimation is deposition or desublimation, in which a substance passes directly from a gas to a solid phase. Sublimation has also been used as a generic term to describe a solid-to-gas transition (sublimation) followed by a gas-to-solid transition (deposition). While vaporization from liquid to gas occurs as evaporation from the surface if it occurs below the boiling point of the liquid, and as boiling with formation of bubbles in the interior of the liquid if it occurs at the boiling point, there is no such distinction for the solid-to-gas transition which always occurs as sublimation from the surface. Phase diagram of this process is represented on Fig. 10 [28].

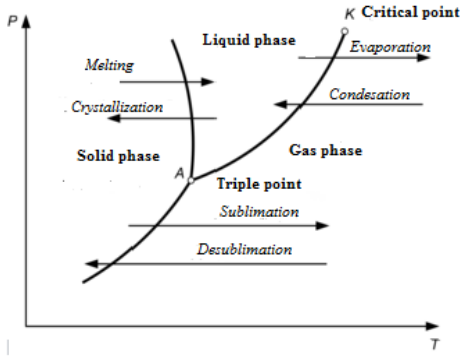

Fig10. *First order phase transitions in the thermodynamic phase diagram [28].*

For the estimation the depth of ablation per pulse next phenomenological formula [8] is used

$$d(F) = \frac{1}{\alpha_{eff}} \ln \frac{F}{F_{th}}, \tag{3}$$

where $d(F)$ is the ablation rate per pulse, α_{eff} is effective absorption index, F is the radiation fluence, F_{th} is the ablation threshold fluence Stafe M., Marcu A., Puscas N. N. are defined as minimum fluence where the onset ablation may be observed [8].

Roughly speaking the laser-induced sputtering may be represented as shock sublimation too. But in this case we must use methods of modeling, which are connected with the intensity of the incident particles flow.

The process of scattering light in solid may be represented in the approximation of short-range action representation. When quantum energy $h\nu >> E_a$, where E_a – the threshold energy of ionization (a disruption) of proper chemical bond, then cascades of collisions (second order effects of scattering ionized electrons) are created. It may be cause of the creation of displacements of atoms (ionic subsystem of crystal). These damages may be having another nature as classic defects.

Simple representation of cascade the ionization may be represented in the next form [27]. Full number of dangling (disrupted) bonds, which are created of the beginning photon, may be determined at next way. This number is depended from quantum energy $h\nu$ and has name cascade function N($h\nu$).

Methods radiation physics of status solid (RPSS) were adapted to the chemical bonds because processes of Relaxed Optics are softer as processes of RPSS [23, 27].

According to this theory trace of full loss energy of photon ($E_m(L) = h\nu$)

$$L = \frac{2}{\sigma_0 N_0} \ln \frac{h\nu}{E_g}. \tag{4}$$

Full number of ionized (disrupted) chemical bonds at trace L is equalled [23, 27]

$$n = n_l L = 2 \ln \frac{h\nu}{E_a}. \tag{5}$$

Third is average distance between two scatterings

$$l_0 = \frac{1}{\sigma_0 N_0}. \tag{6}$$

Radius of sphere of full interaction photon with matter (for isotropic case) may be determined as [23, 27]

$$r_K = \frac{1}{\sigma_0 N_0}\sqrt{2\ln\frac{h\nu}{E_g}}. \qquad (7)$$

The estimations for the absorption Ruby laser irradiation $(h\nu = 1,78eV)$ in *InSb* for room temperature give next values $L = 53.5\dot{A}$, n = 4.6, , $l_0 = 11,7\dot{A}$ and $r_k = 25,2\dot{A}$ [23].

Time and energy characteristics of processes interactions Ruby-laser radiation with indium antimonite may be estimated with the help of next way. In further we'll use two-dimensional representation of crystal lattice *InSb* [[23, 24]. Bond 1 is corresponded to band gap and has value 0,18 *eV*, bond 2 – 1,95 *eV* and bond 3 – 2,15 *eV* [23, 24].

Method of the estimation of level of saturated excitation of proper chemical bonds may be used for the selection of optimal regime for optical pumping of semiconductor laser [23, 24] and for creation stable *n*–*p*-junctions on semiconductors [23, 24] and for the creation layers with new phases, including nanostructures [23, 24].

For these crystals the energy of these bonds are equaled the energy of band gap E_g (0,18 *eV* for *InSb* at room temperature). In two-dimensional lattice [23, 24] this bond is signed as 1. For this bond ions *In* and *Sb* are placed on minimal distance (the sum of proper covalent radiuses). Other chemical bonds in this crystal symmetry have more long sizes. With geometrical point of view in crystal direction {111} the cross section of effective interaction the light quantum with bond 1 is more effective than for direction {110}. The angle among bond 1 and direction {110} is 37,5°. Quanta of ruby laser in linear regime of the irradiation are not interacted with another bonds practically because it energies are less than energy of this bond. The correlation of effective square of bond 1 for directions {110} and {111} is explained the proper experimental data (oriental effect of creation donor centers by Ruby-laser irradiation [23]).

Energy density, which was required for the excitation of "band gap" bonds, is equalled

$$E_1 = 2h\nu\frac{3}{4\pi r_k^3}, \qquad (8)$$

factor 2 is included the large reflection of irradiation from surface of indium antimonite. For *InSb* $E_1 = 8,6\,J/cm^3$. Next phase of excitation is the ionization second valence bonds with energy 1,95 *eV* (for two-dimensional representation of crystal lattice *InSb*, []). With including first processes $r_{K2} \approx 4,5\dot{A}$ for our second process. Therefore

$$E_2 = 2h\nu\frac{3}{4\pi r_{k2}^3}. \qquad (9)$$

For *InSb* $E_2 = 1510\,J/cm^3$ [23, 24]. Further increasing of intensity the radiation lead to the ionization third valent bond with energy 2,15 *eV*. The regime of saturation of its excitation lead to the melting of irradiated semiconductor. For the *InSb* this value is $E_{3s} = 0,16\,J/cm^2$ [23, 24].

Energy of "disruption" of third chemical bonds is equaled $E_{d3} = N_1 E_3 = 4816\frac{J}{cm^3}$.

The question of stability of receiving layer may be explained as increasing of relaxation time of firstly photoexcitations [23, 24].

The estimations of relaxation times with help this method [23, 24] are rough and approximate because it isn't included the collective dynamical processes (heating, melting and other).

The hierarchy of values these times is corresponded to the experimental data of the formation laser induced donor centers in nanosecond Ruby-laser irradiated of indium antimonite [23, 24].

This method may be used for the calculations and estimations of experimental data of irreversible interaction laser irradiation with other semiconductors.

The use of the disruption two bonds in two-dimensional representation crystal lattice of sphalerite for the creation stable irreversible state in *InSb* may be "pulse" criterion of the creation underthreshold defects in the regime of saturated excitation two types of chemical bonds [23, 24]. The disruption three bonds in this representation is the addition to famous Lindemann criterion of material melting [23, 24]. The famous Haken problem (chaotization of laser radiation) may be explained as second-order recrystallization of irradiated semiconductor [23, 24].

Increasing of intensity of laser irradiation more as threshold of saturation one or more chemical bonds may be caused of appearance new phases. First effect was named a metallization of semiconductor [23]. It can have nonequilibrium and irreversible nature. In irreversible case it may be caused phase transitions of diffusive type.

For the explanation these results we can use the theory of phase transitions and methods of irreversible kinetics.

Results of its modeling allow uniting in one system basic effects of interaction laser irradiation with crystals.

These models may be used for the case of nanosecond Ruby-laser irradiation (wavelength 694.7 *nm*, pulse duration 20 *ns*).

For case of CO_2-laser irradiation (wavelength 10. μm, stationary regime) we can use this model too. But in this case main nature of generation the sputtering (ablation) processes are thermal. Therefore, the processes of reabsorption and reradiation are basic for the heating the irradiated matter. For surface sublimation of indium antimonide, it is sufficient to break two of the three bonds (two-dimensional model).

The explanation of experimental data of sublimation indium antimonite after stationary CO_2 laser irradiation may be made with help two-dimensional lattice structure of sphalerite modification this crystal [23, 24]. Sum of energies of three chemical bonds in this picture is equaled 4.38 *eV* [2]. Density of energy three chemical bonds of *InSb*, which is necessary for the disruption these three bonds, is equaled 9587.2 $J \cdot cm^{-3}$ [2, 23, 24]. For volume of our sample with thickness 0.8 mm we have energy 69.02 *J*. Effective surface of irradiation is 3.5325 times more and therefore effective energy of irradiation must be 243,8315 *J*. But real energy of irradiation was changed from 600 to 1500 *J*. The radiation utilization rate was 0.16 – 0.4. Such a large value of the absorption coefficient is due to multiphoton absorption and a large spread in the bond energies of indium antimonide (0.18 *eV*, 1.95 *eV* and 2.15 *eV*), as well as the heating of the crystal. For sublimation from the surface, it is sufficient to break the first two bonds in the absorption saturation mode. This process is represented first cascade process according to our classification of introduction of this paper. Main mechanisms of heating are multiphotonic, reradiation and reabsorption processes [2, 23, 24].

With point of view of physics status solid the chain of possible irreversible formations in *InSb* after Ruby laser irradiation with increasing of level of irradiated intensity may be next: excitons; multiexcitons; excitons drops; diffusive, martensite or diffusive–martensite phases; destruction and evaporating materials [21, 23]. These transformations may be modelled with help of various physical theories.

The problem of CO_2-laser-induced sublimation of indium antimonite may be resolved in short-range action approximation as cascade processes another nature [2].

The main role is played by multiphoton processes of absorption and re-emission. So to break the bond 1 of InSb (two-dimensional diagram) requires 2 photons of CO_2 laser radiation, bonds 2 – 17 photons, and bonds 3 – 19 photons. Therefore, the kinetic chemical mechanism of ablation is unlikely in this case, although it affects the heating kinetics. It's just that most of the absorbed energy is converted into heat. However, since the energies of chemical bonds according to two-dimensional lattice are very different from each other, this causes the sublimation of the irradiated material, by passing its melting.

It should be noted that between two-photon and seventeen-photon absorption, intermediate absorption mechanisms with a smaller number of photons can also occur. And since there are non-radiative resonant transitions, it seems that we have non-radiative relaxation, which leads to heating of the irradiated material.

In this case, it is necessary to evaluate the time processes of laser-induced sputtering (ablation) differently. We must determine the time at which the irradiated substance is at a temperature above or equal to the sublimation threshold temperature.

Thus this representation of the modeling dangling bonds, which are created with help laser irradiation, is very effective method. It allows including in consideration effects of equilibrium, nonequilibrium and irreversible relaxations.

The main difference between nanosecond and femtosecond ablation is analyzed [2, 15].

For nanosecond regime of irradiation we have next chain of processes: heat of irradiated matter – melting – evaporation. In this case the generation of shock waves is possible too. For femtosecond regime of irradiation the melt zone and shock waves are absented [2, 15]. Strictly speaking, this explanation is rather conditional because we must take into account the efficiency of using laser radiation for photoinduced (photochemical) irreversible processes, in other words, how many chemical bonds can be broken by one photon. As a result, the relaxation time increases.

Comparative visual analysis of Figs. 1 and 2 with Fig. 5 shows that the results shown in the first two figures correspond to the phenomena of the third type, and Fig. 5 – the second type processes of our classification.

For the estimation the differential photochemical efficiency of using laser radiation for photochemical irreversible processes we can use next formula for the determination of number of broken chemical bonds per one photon n [23, 24]

$$n = 2\ln\frac{h\nu}{E_a}, \tag{5a}$$

where $h\nu$ – photon energy; E_a – energy of activation (broken) of corresponding bond.

So, for the case of the irradiation *InSb* by Ruby laser pulses (photon energy 1.78 *eV*) we have for the first bond of two-dimensional lattice (E_{1InSb} = 0.18 *eV*). These crystals are direct-gap, so the band gap is equal to the energy of the minimum chemical bond [23, 24]. Therefore, n_{InSb} ~ 4.6 bonds/photon. For case of irradiation *Si* (E_a ~ 1.6 *eV*) by irradiation of eximer laser pulses (photon energy 5 *eV*) we have n_{Si} ~ 2.3 bonds/photon. These conditions allow increasing the lifetime of excited states and therefore the heating of irradiated matter may be negligible compared to direct photoionization, including phase transformations of the irradiated material.

Formula (5a) has large value for the crystals. For the polymers, glasses and amorphous media this condition may be represented as

$$h\nu > E_a. \tag{10}$$

These conditions may be supplemented by the multiphoton absorption conditions. But for the silicon we have more intensive generation of laser-induced surface structures for nanosecond irradiation by eximer *KrF*-laser as for femtosecond irradiation of laser with photon energy 1.55 *eV* [21].

For the determination the differential photochemical efficiency in addition to formulas (5a) and (10), the excitation saturation procedure is of great importance.

In other words, for successive n-photon absorption for the next absorption event, the medium must be in the excited state that was obtained during previous absorptions.

The concept of differential photochemical efficiency is connected related to the photochemical equivalent law [29]. This law for sufficiently weak radiation fluxes was derived by A. Einstein on the basis of thermodynamic reasoning.

In contrast to A. Einstein's model, we have more intense radiation fluxes and, depending on the irradiation conditions, we can have such nonlinear optical phenomena as quantum splitting, multiphoton absorption, etc.

According to [26] photoionization processes should be considered as chemical reactions.

For the research dynamics of chemical reactions we must have possibility to receive and use ultra short times. For resolution of these problems femtochemistry was created [30].

Femtochemistry is a branch of physical chemistry that studies chemical reactions over very short time intervals, on the order of femtoseconds (hence the name). For his work in this area, A. Zewail received the Nobel Prize in Chemistry in 1999 [30]: "for real-time studies of chemical reactions using femtosecond spectroscopy." The main result of the work is that it became possible to observe the flow of elementary chemical reactions "in real time" and thereby created a new branch of chemistry - femtochemistry, which studies chemical processes in the femtosecond time range (10^{-15} – 10^{-12} seconds). Elementary reactions are studied in a special branch of chemistry – chemical dynamics. The main task of chemical dynamics is to determine the structure of the transition state and trace the dynamics of its formation and decay in real time.

It should be noted that for the irradiation of indium antimonide by ruby laser radiation, the lower limit of the time interval is 10^{-7} – 10^{-5} seconds. From this point of view, femtochemistry can also be considered as a branch of Relaxed Optics [26].

The model of laser-induced two-photom polymerization (TPP) and two-photon absorption (TPA) is represented in [31]. This theory is synthesis of the methods of Nonlinear Optics and chemical-physical kinetics.

This model can be adapted and used to simulate the interaction of stationary CO_2-laser radiation with indium antimonite. Moreover, from an energetic point of view, the main processes that lead to the sublimation of the material are of a thermal nature.

Cascade model in the regime of saturation of excitation for explanation of laser-induced sputtering (sublimation) may be used [21]. We are demonstrating this model on *Si* and *Ge* examples.

Results of calculation of volume densities of energy, which are necessary for breakage of proper number of bonds in regime of saturation of excitation, are represented in Table 1 [2, 21].

Table1. *Volume density of energy I_{vi} (10^3 J/cm^3), which is necessary for the breakage of proper number of chemical bonds in the regime of saturation of excitation in Si and Ge [2].*

	I_{v1}	I_{v2}	I_{v4}	I_{v5}
Si	12,8 – 14,4	25,6 – 28,8	51,2 – 57,6	63 – 72
Ge	6,3 – 8,4	12,6 – 16,8	25,2 – 33,6	31,5 – 42

It conceded that energies of all chemical bonds for elementary lattice are equivalent (*Si* and *Ge* are pure homeopolar semiconductors) [21]. For silicon energy of covalent bonds *Si-Si* are equaled 1,6–1,8 *eV*; for germanium energy of covalent bonds *Ge–Ge* are equaled 1,2–1,6 *eV*. Minimal values of these energies are corresponded of Pauling estimations. These values are corresponded the energy on one coordination number: according to radiation physics of status solid Seitz energy of creation one radiation defect in silicon is equal 12,7 *eV* for diamond lattice [27].

The values of molar volume, density of atoms, densities of sublimation energy and value of siublimation energy on one atom for *Si, Ge* and *Fe* are represented in Table 2 [2].

Table2. *Thermodynamical characteristics, which are necessary for the sublimation silicon, germanium and steel [2].*

Material	V_{mol} , cm^3	n_i, cm^{-3}	E_{subl}, kJ/cm^3	E_{atomi}, eV
Si	12,18	$5\cdot10^{22}$	36	4,50
Ge	13,64	$4\cdot10^{22}$	27	4,20
Fe	7,14	$8{,}4\cdot10^{22}$	56	4,16

Comparative analysis of estimated data from Table 1 and Table 2 for silicon and germanium, show that for sublimation in thermodynamic approximation value energy per atom is equaled 0,5 – 0,57 value of Seitz energy approximation (for I_{v5}). For the surface laser-induced sublimation breaking 5 bonds out of 8 is enough. But this estimate is valid only for an intense laser radiation flux, which makes it possible to break five chemical bonds out of eight in the regime of radiation saturation.

In the multipulse irradiation regime, we have a whole cascade of successive phase transformations from higher-symmetry phases to low-symmetry phases (Fig. 1 – Fig. 3). This explains the similarity of the formed structures Fig. 3. Crater walls of Fig. 1 c) and Fig. 2 have hedgehog structuring. But due to the inhomogeneity of irradiation, the tops of hedgehog-like microcones begin to evaporate, so their tops resemble shark mouths (Fig. 3, right). In this case, sublimation from the solid phase occurs. This explains the shape form of the craters Fig. 1 c).

The model of the plasma torch, which is formed during pulsed ablation, is given in [16].

Optical breakdown in gases occurs through an electron avalanche, driven by heating of free electrons by a strong laser electric field via multiple collisions with gaseous neutral species at a rate ν (inverse Bremsstrahlung absorption) [16]. The avalanche multiplication of free electrons takes place when their kinetic energy becomes comparable to the first ionization potential J_p of the species, at the time increment r_{ion}, which is a function of laser intensity and wavelength, as well as of gas thermo-dynamic parameters (pressure P and temperature T) [16]. Then, the development of the electron avalanche is assumed to be terminated (at least, in rarefied gases) by complete gas ionization [$N_e(\infty) \approx N$] after a number of carrier duplications steps with the overall ionization time T_{ion} proportional to the product of τ_{ion} and the natural logarithm of the ratio of the gas density N at the given P and T, and initial electron density $N_e(0)$ (usually, $N_e(0)$ is arbitrarily taken equal to 1 cm^{-3}, i.e., under the normal air conditions—atmospheric gas pressure $P_0 = 1$ bar, $T_0 \approx 300$ K, $N_0 \sim 10^{19}$ cm^{-3} – $T_{ion} \approx 40\ \tau_{ion}$) [16]. As a result, in this simple model, neglecting diffusion and recombination of free electrons, as well as their attachment to neutral atoms to form negative ions, the break-down threshold intensity I_{break} is defined as the laser intensity value providing complete ionization of the gas exactly at the end of the heating laser pulse [16]

$$I_{break} = \frac{40\pi c J_p}{\tau_{las} \nu R_{elas}^2}\left(1+\frac{\nu^2}{\omega_{las}^2}\right), \tag{11}$$

where c is the electromagnetic velocity in vacuum, $R_e = e^2 / m_e c^2 \approx 3 \cdot 10^{-15}$ m is the classical radius of electron of the mass m_e and charge e, $\omega_{las} = 2\pi c / h_{las}$ is the laser frequency. At the normal conditions for visible laser wavelengths and nanosecond pulses the term in square brackets in Eq. (11) is ≈ 1, providing wavelength- and pulse-width-dependent optical breakdown thresholds $I_{break}[GW/cm^2] \approx 10^3 / \lambda_{las}^2 \tau_i$ with the laser wavelength in microns and pulse width in nanoseconds [16].

However, at higher gas pressures the I_{break} value rapidly (as P_0 / P) decreases, comparing to the atmospheric pressure threshold $I_{break,0}$, due to more frequent electron-neutral particle collisions and the resulting higher heating rate. This decrease occurs until $\nu(P)$ becomes equal to ω_{las} at certain pressure $P_{min} = P_0[\omega_{las} / \nu(P_0)]$, but then the breakdown threshold starts to increase monotonically as P/P_0 [16]. The overall pressure dependence for I_{break} is described as follows [16]:

$$I_{break}(P) = I_{break,0}\left[\frac{P_0}{P} + \frac{P}{P_0}\left(\frac{\nu(P_0)}{\omega_{las}}\right)^2\right], \tag{12}$$

exhibiting the minimum exactly at P_{min}.

Importantly, optical breakdown in ablative plumes in front of solid or liquid targets can be easily distinguished from that one in the ambient air atmosphere, since the plume breakdown intensities are by two or three orders of magnitude lower [16]. Despite a number of secondary effects [16], including electron and ion emission from the targets, the increase of the near-surface laser intensity due to the surface reflection, local laser electric field enhancement due to surface roughness, the lower average ionization energy for hot ablation products, the main factor underlying nanosecond laser-induced optical breakdown in vapor plumes, is consid-ered to be high vapor pressure of ablation products (in excess of 10^2 bar) [16]. For the near-critical surface phase explosion, raising the plume pressure to the near-critical pressure magnitudes (~10^3 bar), which are favorable for optical breakdown at lower I_{break} [16], the optical breakdown becomes directly related to the phase explosion threshold I_{PE}. Moreover, though the equation of state for the near-critical vapor differs significantly from that of ideal gas ($P \sim NT$), in lieu of a multiphase (vapor-droplet) character of ablation products after the phase explosion [16], the ideal-gas equation can still be considered as a good approximation to account for the vapor density (pressure) effect on I_{break} under these conditions. In this approximation, for the given plume pressure P the high (near-critical) temperature of the ablation products will shift $I_{break}(P)$ curve to higher pressures by an order of magnitude. Furthermore, the high plume temperature provides the corresponding high initial electron density $N_e(0)$ in the plume (~$N \cdot \exp[-J_p/k_B T_{cr}]$) with a minor con- tribution of thermionic emission, providing complete ioniza-

tion [$N_e(\infty) \approx N$] of the plumes in the time period proportional to ($J_p / k_B T_{cr}$). The slightly modified $I_{break}(P)$dependence for the near-critical dense ablation plumes reads as

$$I_{break}(P,T) = \frac{\pi c J_p}{\tau_i \nu(P_0) R_e \lambda_{las}^2} \left(\frac{J_p}{k_B T_{cr}} \right) \left[\frac{P_0}{P} + \frac{P}{P_0} \left(\frac{\nu(P_0)}{\omega_{las}} \right)^2 \right], \quad (13)$$

including all the abovementioned important factors ($J_p/k_B T_{cr}$), spectral and pressure ones [16], which affect optical breakdown of vapor under near-critical laser-heating conditions.

The latter equation was used in this work in calculations of $I_{break}(P)$ values for the employed 25 *ns*, 532 nm laser pulses, considering, as a zero-order approximation, the near-critical carbon vapor of the atomic (C_1) species [16] with the evaluated collision cross-section $\sigma_{ibs} \approx 1.8 \times 10^{-20}$ m^2 and first ionization potential $J_{p,1} \approx 10.9$ eV [16], and the near- critical phase explosion temperature $\approx 7 \times 10^3$ K [16]. The calculated $I_{break}(P)$ curve [16] exhibits the minimal I_{break} value of ≈ 2 GW/cm^2 at $P_{min} \approx 4.9 \times 10^3$ bar, in poor agreement with our experimentally observed plasma formation threshold $I_{plas} \approx 0.25$ GW/cm^2 (Figs. 8 – 9) and corresponding recoil and plume pressures P_{rec}, $P_S \approx 1 \cdot 10^3$ bar(Fig. 9 a)) see two or three orders of magnitude higher I_{break} values measured so far for much lower gas pressures [16].

The possible discrepancy between the calculated and measured magnitudes I_{break} and I_{plas}, respectively, by the factor of 10 may result from our experimental uncertainties, e.g., neglecting the intermediate electronically excited species in the carbon plumes, transient surface reflection, thermionic emission, the rather rough estimates for σ_{ibs} related to the rather extensive carbon cluster abundance for the near-critical carbon vapor composition (predominantly, C_1 and C_3 species [16]), as well as from the very approximate character of the ideal gas equation used in the near-critical thermodynamic region (i.e., the vapor density will be higher in the region, approaching to the liquid carbon density [16]). As an example, according to our calculations, the increase of σ to $\approx 5.4 \cdot 10^{-20}$ m^2 for C_3 species ($J_{p,3} = 12$ eV), which we also present (even predominating [16]) in the near-critical region, would yield in much lower and closer $P_{min} \approx 1.6 \cdot 10^3$ bar, but in almost the same $I_{break} \approx 2.4$ GW/cm^2 [16].

These results indicate that the variation of the vapor composition affects presumably $\nu(P_0)$ (through σ_{ibs}), significantly changing $P_{min} = P_0[\omega_{las}/\nu(P_0)]$. Apparently, the breakdown threshold I_{break} can be influenced mostly by changes in J_p (e.g., for large graphitelike carbon nanoclusters C_∞, simultaneously emerging as a significant high-mass fraction of a vapor-droplet mixture of ablation products during such near-critical phase explosions [16], their first ionization potential $J_{p,\infty}$ may become as low as the work function of graphite ≈4.6 eV [16]), reducing the threshold by the factor of $(J_{p,\infty}/J_{p,1,3})^2 \sim 10$ and the corresponding magnitude P_{min} by the factor of $(J_{p,\infty}/J_{p,1,3}) \sim 3$. However, despite of the reasonable agreement between I_{plas} and I_{break} (Fig. 5.18), when impact ionization of the high-mass carbon nanoclusters C_∞ is presumably taken in to account, the rather high electron affinity values ($\approx J_{p,\infty}$) for such car-bon nanoclusters [16] make them poor scattering partners in electron-neutral collisions due to electronic attachment, so more efficient laser heating of electrons seems to occur in their collisions with the most abundant C_3 species.

Spatiotemporal dynamics of optical breakdown and plasma in the laser plumes was researched in [16].

From existence of the optical breakdown threshold intensity $I_{break}(P^*)$, which determines of plasma formation, we can introduce the initial radius W_{break} of the breakdown plasma for the incident focused Gaussian beam

$$W_{break}(I_{peak}) = w_o \sqrt{\ln\left(\frac{I_{peak}}{I_{break}(P^*)} \right)} \quad (14)$$

and duration of optical breakdown in the vapor, $T_{break} = 2t^*$, in the explicit form

$$T_{break}(I_{peak}) = \tau_i \sqrt{\ln\left(\frac{I_{peak}}{I_{break}(P^*)} \right)}. \quad (15)$$

Formulas (14) and (15) allow estimating experimental data of Fig. 9 b).

For more detailed modeling, it is necessary to use the phase diagrams of the irradiated compounds. If for simple compounds (silicon and germanium) we have a relatively small number of intermediate phases, then for more complex compounds, including two- and more-component inorganic compounds and polymers, the number of phases can be change from tens to even hundreds. Therefore, in this case, further research is needed.

Promising areas of research into laser-induced sputtering (ablation) of a substance include the following questions: the influence of irradiation conditions on the formation of direct photochemical transformations, plasma generation, and the formation of thermal fields. It is also advisable to study in more detail the conditions for the occurrence of laser-induced melting and sublimation of a substance, as well as the formation of near-surface plasma, which occurs during sputtering.

From an applied point of view, to determine the effect of interference and diffraction processes on ablation, as well as the conditions for the disposal of a sprayed substance and other geometrical conditions of laser irradation.

4. Conclusion

1. System analysis of the problem of laser-induced sputtering is represented. It was shown that three types processes may be realized.

2. Thermodynamical analysis of these processes is represented too.

3. Role of chain processes and conditions of absorption the optical radiation on generation the surface sputtering are discussed.

4. Physical-chemical models for various regimes of irradiation are observed.

5. Spatiotemporal dynamics of optical breakdown and plasma in the laser plumes is researched.

References

[1] Hadlund R. F., Kelly R. (1993) Electronic Processes in Sputtering by Laser Beams. Fundamentals Processes in Sputtering of Atoms and Molecules, Symposium on the Occasion of the 250th Anniversary of the Royal Danish Academy of Sciences and Letters Copenhagen, 30 August - 4 September, 1992 Invited Reviews Edited by Peter Sigmund. Munksgaard • Copenhagen, 527 – 592.

[2] Trokhimchuck P. P. (2021) Modelling of the elionic-induced sputtering (sublimation) of matter. Applied Questions of Mathematics modeling, vol. 4, is. 2.1, 234-244.

[3] Trokhimchuck P. P. (2022) On the issue of modeling elyon-induced sputtering./ Proc. all-ukrainian seminar "III Spring readings of Anatoliy Vadimovich Svidzinskyi". Ed. Trokhimchuck P. P., Shvalikovskyi D. M. Vezha-Print, Lutsk, 34-37 (In Ukrainian)

[4] Laser ablation and its applications. Ed. Phipps C. (2010) Springer Verlag, Berlin

[5] Laser ablation. Principles and applications. Ed. Miller J. C. (1994) Springer Verlag, Berlin

[6] Pulsed laser ablation. Advances and applications in nanoparticles and nanostructuring thin films. Ed. Mihailescu I. N., Carcato A. P. (2018) Pan Stanford Publishing Pte. Ltd., Singapore

[7] Stafe M., Marcu A., Puscas N. N. (2014) Pulsed laser ablation of solids. Springer, Heidelberg

[8] Advances in Laser Materials Processing Technology, Research and Applications. Ed. Lawrence J. R. (2018) Elsevier Publishing, Amsterdam

[9] Anisimov S. I., Lukyanchuk B. S. (2002) Selected problems of the theory of laser ablation. Usp. Phys. Nauk, vol. 172, is. 3, 301 – 333 (in Russian)

[10] Baudach S., Bonse J., Kautek W. (1999) Ablation experiments on polyimide with femtosecond laser pulses. Appl. Phys. A, vol. 69 [Suppl.], S395 – S398

[11] Bobytski Ya. V., Matviyishyn G. L. (2015) Laser technologies. Part 1. Lvivska Politekhnika Publishing, Lviv (in Ukrainian)

[12] Bobytski Ya. V., Matviyishyn G. L. (2020) Laser technologies. Part 2. Lvivska Politekhnika Publishing, Lviv (in Ukrainian)

[13] Costache E., Kouteva-Anguiriva S., Reif J. (2004) Sub-damage-threshold femtosecond laser ablation from crystallic Si: surface nanostructures and phase transformations. Appl. Phys. A, vol. 79, 1429 – 1432.

[14] Dupliak I., Li F., Feng F. Micro-hole drilling of stainless steel using short pulse laser./ Proceedings Third International Conference "Actual Problems of Fundamental Science" dedicated to the memory of Anatoliy V. Svidzinskyi, I – 5 June, Lake "Svityaz'", 2019. Lutsk: Vezha-Print, 2019. – P. 42-44.

[15] Ionin A. A., Kudryashov S. I., Seleznev L. V. (2010) Near-critical phase explosion promoting breakdown plasma ignitionduring laser ablation of graphite. Phys. Rev E., vol.82, 016404, 9

[16] Lasers in Materials Science. Eds. Castillejo M., Ossi P. M., Zhigilei L. (2012) Springer Series in Materials Science, Volume 191. Springer Verlag, Stutgart

[17] Veyko V. P., Libenson M. N., Chervyakov G. G., Yakovlev E. B. (2008) Interaction laser irradiation and matter. Force optics. Phyzmatlit, Moscow (In Russian)

[18] Vorobyov A. Ya., Guo Ch. (2011) Reflection of femtosecond laser light in multipulse ablation of metals. J. Appl. Phys., vol. 110, Is. 4, 043102, 1 – 9.

[19] Mishra S. (2015) Laser Beam MicroMachining. Optics and Lasers in Engineering, vol. 73, 89-122.

[20] Philips J. C. (1981) Metastable honeycomb model of laser annealing. Journal of Applied Physics, vol. 52, is.12, 7397–7402.

[21] Trokhimchuck P. P. (2020) Relaxed Optics: Modeling and Discussions. Lambert Academic Publishing, Saarbrukken

[22] Trokhimchuck P. P. (2018) Some Problems of Modeling the Volume Processes of Relaxed Optics. IJARPS, vol. 5, is. 11, 1-14.

[23] Trokhimchuck P. P. (2012) Problem of saturation of excitation in relaxed optics. JOAM, vol. 7, is. 3-4, 363-370.

[24] Trokhimchuck P. P. (2016) Relaxed Optics: Realities and Perspectives. Lambert Academic Publishing, Saarbrukken

[25] Trokhimchuck P. P. (2021) Recent Research and Development Satus of Relaxed Optics and Laser Technology: A Review. Optics and Photonics Journal vol. 11, is. 7, 210-263.

[26] Trokhimchuck P. P. (2020) Role Physical-Chemical Processes in the Generation of Laser-Induced Structures. In: Research Trends in Chemical Sciences, ed. Ashok Kumar Acharya, vol. 11, ch.6, AkiNik Publications, New Delhi, 109-140.

[27] Trokhimchuck P. P. (2007) Radiation Physics of Status Solid. Vezha, Lutsk (In Ukrainian)

[28] Whitten K. W., Gailey K. D., Davis R. E. (1994) General chemistry with qualitative analysis. Saunders College Publishing, Rochester

[29] Einstein A. (1913) Deduction thermodynamique de la loi de l'equivalence photochimique. J. Phys., ser. 5, vol. 111, 277-282 (in French)

[30] Zewail A. H. (1996) Femtochemistry: Recent progress in studiesand control of reactions and their transitions states. J. Phys. Chem., vol. 100, No.31, 12701 – 12724

[31] Zheng C., Hu A., Chen T., Oakes Ken D., Liu S. (2015) Femtosecond laser internal manufacturing of three dimensionalmicrostructure devices. Applied Physics A, vol. 121, is. 1, 163-177

Citation: *Petro P. Trokhimchuck (2022) "Laser-Induced Sputtering (Ablation) of Matter: Retrospective and Perspective " International Journal of Advanced Research in Physical Science (IJARPS) 9(4), pp.19-33, 2022.*